

## **Q1 Connectometry: A statistical approach harnessing the analytical potential 2 of the local connectome**

**Q2 Fang-Cheng Yeh <sup>a,\*</sup>, David Badre <sup>b</sup>, Timothy Verstynen <sup>a,\*</sup>**

<sup>4</sup> *Department of Psychology, Carnegie Mellon University, PA, USA*

<sup>5</sup> *Department of Cognitive, Linguistic and Psychological Sciences, Brown University, RI, USA*

<sup>6</sup>

### 7 ARTICLE INFO

#### 8 Article history:

Received 18 August 2015

Accepted 19 October 2015

Available online xxxx

#### 12 Keywords:

Connectome

Connectometry

Diffusion MRI

Diffusion spectrum imaging

q-Space diffeomorphic reconstruction

Generalized q-sampling imaging

Quantitative anisotropy

33

34

35

36

### 38 Introduction

The human connectome refers to the map of connections between distinct cortical regions (Akil et al., 2011; DeFelipe, 2010; Seung, 2011; Turk-Browne, 2013), where connectivity is typically quantified using functional (e.g., functional MRI, electrophysiological approaches) (Biswal et al., 2010; Dolgin, 2010; Fornito et al., 2015; Honey et al., 2009; Johansen-Berg et al., 2004) or structural measurements (e.g., diffusion MRI) (Craddock et al., 2013; Hagmann et al., 2010b; Pestilli et al., 2014; Wedeen et al., 2012). Diffusion MRI is currently the most popular method for measuring the structural connectome in humans. It allows for mapping macroscopic end-to-end connections between parcellated gray matter targets using a fiber tracking algorithm (Sporns, 2013; Wedeen et al., 2012), and the streamline count of the connections can be used as a measure of global connectivity in several connectomic studies (Fig. 1a) (Bullmore and Sporns, 2009; Hagmann et al., 2008; Hagmann et al., 2007; Hagmann et al., 2010b; Sporns, 2014a, b). These structural connectomic approaches have used connectivity matrices to represent the graph structure of connectome, and graph-theoretic measures were estimated from these matrices to

### A B S T R A C T

Here we introduce the concept of the local connectome: the degree of connectivity between adjacent voxels within a white matter fascicle defined by the density of the diffusing spins. While most human structural connectomic analyses can be summarized as finding global connectivity patterns at either end of anatomical pathways, the analysis of local connectomes, termed connectometry, tracks the local connectivity patterns along the fiber pathways themselves in order to identify the subcomponents of the pathways that express significant associations with a study variable. This bottom-up analytical approach is made possible by reconstructing diffusion MRI data into a common stereotaxic space that allows for associating local connectomes across subjects. The substantial associations can then be tracked along the white matter pathways, and statistical inference is obtained using permutation tests on the length of coherent associations and corrected for multiple comparisons. Using two separate samples, with different acquisition parameters, we show how connectometry can capture variability within core white matter pathways in a statistically efficient manner and extract meaningful variability from white matter pathways, complements graph-theoretic connectomic measures, and is more sensitive than region-of-interest approaches.

© 2015 Elsevier Inc. All rights reserved.

32

study how topological patterns varied along experiment-relevant dimensions. However, these “find-difference-in-track” approaches heavily rely on diffusion MRI tractography to quantify end-to-end connectivity. While diffusion MRI tractography has increased in popularity over the last decade, several recent studies have identified critical concerns with the reliability of end-to-end connectivity measurement (Reveley et al., 2015; Thomas et al., 2014). Specifically, fiber tracking algorithms have exhibited limited reliability near the gray matter targets, thus putting into question the reliability of these “find-difference-in-track” methods.

To bypass the limitations of end-to-end fiber tracking, we introduce the concept of the local connectome: the degree of connectivity between adjacent voxels within a white matter fascicle defined by the density of the diffusing spins (Fig. 1b). Since the entire connectome is defined as the complete map of connections in the brain, knowing the local orientation and integrity of the fiber bundles as they run through the core of white matter is just as important as knowing where a bundle starts and stops. In this way the local connectome can be viewed as the fundamental unit of the end-to-end structural connectome, and thus analyzing the local connectomes along fiber bundles may serve as a surrogate for the global end-to-end connectivity analysis. The mapping and analysis of local connectomes, termed connectometry, adopted a “track-difference” paradigm. Instead of mapping the entire end-to-end connectome, connectometry tracks only the segment of fiber bundle that exhibits significant association with the study variable. This is

66

67

68

69

70

71

72

73

74

75

76

77

78

79

80

81

\* Corresponding authors at: Department of Psychology and Center for the Neural Basis of Computation, Carnegie Mellon University, Pittsburgh, PA, USA.

E-mail addresses: [frank.yeh@gmail.com](mailto:frank.yeh@gmail.com) (F.-C. Yeh), [timothyv@andrew.cmu.edu](mailto:timothyv@andrew.cmu.edu) (T. Verstynen).

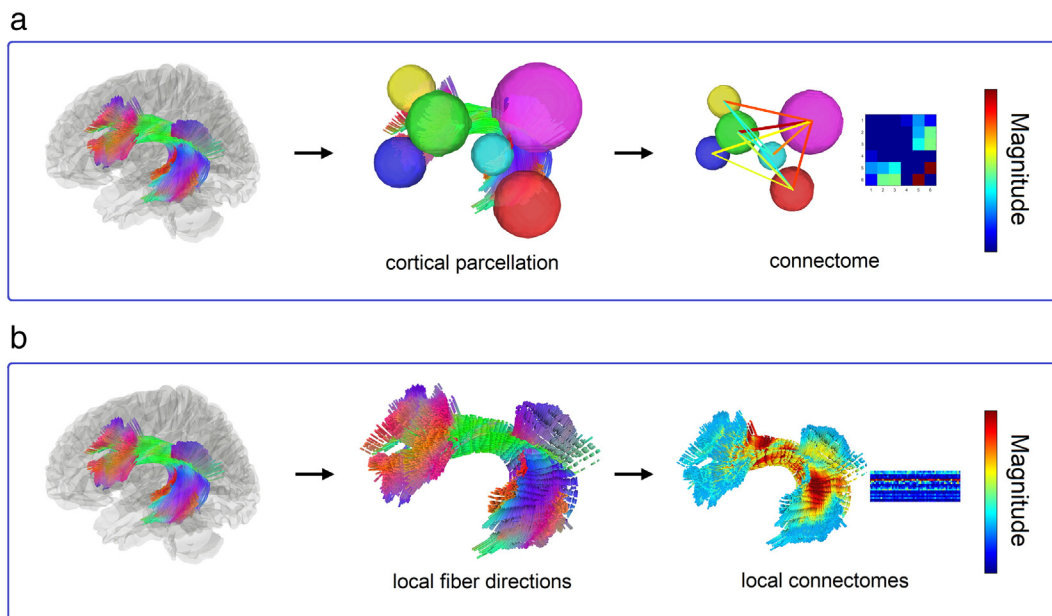


**Fig. 1.** Differences between the global connectome and local connectome. (a) The mapping of human connectome relies on cortical parcellation to define a set of common regions (nodes) for calculating the connectivity measurements (edges). The connectivity can be measured by the number of the connecting tracks or their mean anisotropy value. The final form can be expressed as a symmetric connectivity matrix. (b) The mapping of local connectome utilizes local fiber directions from a common atlas to sample the density of diffusing spins as the connectivity measurement. Multiple measurements can be obtained along the fiber pathways to reveal the change of track compactness within a fiber bundle. The local connectome of a subject can be represented by a row vector, whereas the local connectomes from a group subject can be compiled as a local connectome matrix.

realized by reconstructing diffusion MRI data into a standard template space to map a local connectome matrix from a group of subjects (Fig. 2a). Study-relevant variables are then associated with this local connectome matrix in order to identify local connectomes that express significant associations with the variable of interest (Fig. 2b). These local connectomes are then tracked along the core pathway of a fiber bundle using a fiber tracking algorithm and compared with a null distribution of coherent associations using permutation statistics (Nichols and Holmes, 2002) (Fig. 2c). Permutation testing allows for estimating and correcting the false discovery rate (FDR) of Type-I error inflation due to multiple comparisons. We show how different levels of FDR can be devised to tune the sensitivity and specificity of connectometry for exploratory purposes (high FDR) or confirmatory purposes (low FDR).

We benchmarked the performance of connectometry by replicating a well-established negative association between global white matter integrity and physical obesity (Gianaros et al., 2013; Mueller et al., 2011; Stanek et al., 2011; Verstynen et al., 2013, Verstynen et al., 2012). This was done using two data sets acquired in different imaging

environments and using two different forms of high angular resolution diffusion MRI. By comparing our results against traditional tractography and region-of-interest approaches, we show how connectometry can complement conventional end-to-end connectivity analyses and provide a more nuanced description of variability within core white matter pathways.

## Methods

### Diffusion MRI acquisitions

The first data sample consisting of a total of 60 subjects with no previous history of neurological or mental disorder were scanned on a Siemen's Verio 3 T system in the Scientific Imaging & Brain Research Center at Carnegie Mellon University (abbreviated as CMU hereafter) using a 32-channel head coil. We collected a 50 min, 257-direction diffusion spectrum imaging (DSI) scan using a twice-refocused spin-echo EPI sequence and multiple q values (TR = 9916 ms, TE = 157 ms,

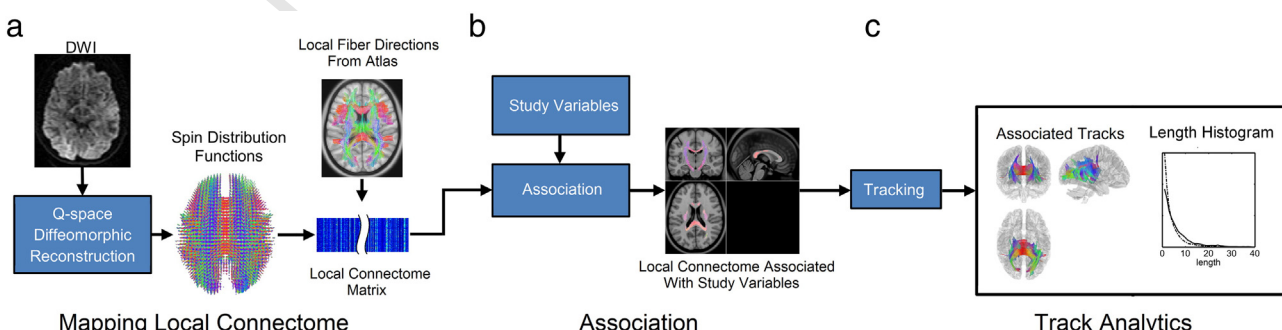


**Fig. 2.** Diagram of the connectometry pipeline. (a) The diffusion data of each subject are reconstructed in a common standard space, and the calculated spin distribution functions are then sampled by the local fiber directions from a common atlas to estimate the local connectome. The local connectome of a group of subjects can be compiled as a local connectome matrix. (b) The local connectome matrix is then associated with study variables using relevant statistical procedures (e.g., using a multiple regression model). (c) The local connectomes that express positive or negative association with the study variable can be tracked along a common pathway to reveal the subcomponents of the fascicles that have significant associations. The length histogram of these subcomponents is calculated, and the statistical inference can be obtained by comparing the findings with a null distribution to estimate the false discovery rate.

voxel size =  $2.4 \times 2.4 \times 2.4$  mm, FoV =  $231 \times 231$  mm, b-max = 5000 s/mm<sup>2</sup>, 51 slices). Head-movement was minimized during the image acquisition through padding supports and all subjects were confirmed to have minimal head movement during the scan prior to inclusion in the template. Another set of 20 subjects with no previous history of neurological or mental disorder was scanned in a Siemens 3 T Tim Trio System at Brown University (abbreviated as BU hereafter). A twice-refocused spin-echo sequence was used to acquire DSI with a 32-channel head coil. The total diffusion sampling direction was 257. The spatial resolution was 2.4 mm isotropic. TR = 9900 ms, and TE = 157 ms. The maximum b-value was 7000 s/mm<sup>2</sup>.

The second data set was from the Human Connectome Project consortium led by Washington University, University of Minnesota, and Oxford University (abbreviated as the WU-Minn HCP). 488 of subjects received diffusion MRI scans. The scan was acquired in a Siemens 3 T Skyra scanner using a 2D spin-echo single-shot multiband EPI sequence with a multi-band factor of 3 and monopolar gradient pulse (Sotiropoulos et al., 2013). The spatial resolution was 1.25 mm isotropic. TR = 5500 ms, TE = 89.50 ms. The b-values were 1000, 2000, and 3000 s/mm<sup>2</sup>. The total number of diffusion sampling directions was 90, 90, and 90 for each of the shells in addition to 6 b0 images. The total scanning time was approximately 55 min.

### 137 Connectometry

138 The diagram of the connectometry method is shown in Fig. 2. As  
139 shown in this overview figure, the diffusion data of each subject are  
140 reconstructed in a standard space using q-space diffeomorphic recon-  
141 struction, and the density of diffusing spins is then sampled by the  
142 local fiber directions from a common atlas to estimate the local  
143 connectome and to construct a local connectome matrix (Fig. 2a).  
144 Then the local connectome matrix is associated with study variables  
145 using relevant statistical procedures (e.g., using a multiple regression  
146 model) (Fig. 2b). The local connectomes that express positive or nega-  
147 tive association with the study variable can be tracked along a common  
148 pathway to reveal the subcomponents of the fascicles that have signifi-  
149 cant associations. The length histogram of these subcomponents is  
150 calculated, and the statistical inference can be obtained by comparing  
151 the findings with a null distribution to estimate the false discovery  
152 rate (Fig. 2c). Each step of the connectometry method is detailed in  
153 the following sections.

### 154 Q-space diffeomorphic reconstruction

155 We reconstructed multiple sets of dMRI data into the Montreal  
156 Neurological Institute (MNI) space using q-space diffeomorphic recon-  
157 struction (Yeh and Tseng, 2011) (QSDR). QSDR satisfied the conserva-  
158 tion of diffusion spins after non-linear spatial transformation and  
159 could be applied to diffusion tensor imaging (DTI), DSI, or multishell  
160 data (Yeh and Tseng, 2011) to calculate a spin distribution function  
161 (SDF) (Yeh et al., 2010),  $\Psi(\hat{\mathbf{u}})$ , an orientation distribution function  
162 defined as the density of diffusing spins that have a displacement  
163 oriented at direction  $\hat{\mathbf{u}}$  during the diffusion time (Yeh and Tseng, 2011):

$$\Psi(\hat{\mathbf{u}}) = |J_\varphi| Z_0 \sum_i W_i(\varphi(\mathbf{r})) \text{sinc} \left( \sigma \sqrt{6Db_i} \langle \hat{\mathbf{g}}_i, \frac{J_\varphi \hat{\mathbf{u}}}{\|J_\varphi \hat{\mathbf{u}}\|} \rangle \right) \quad (1)$$

165 where  $\varphi$  is a spatial mapping function that maps a template space coor-  
166 dinates  $\mathbf{r}$  to the subject's space. The mapping function was calculated  
167 using a non-linear registration between subject anisotropy map and  
168 the anisotropy map in the MNI space (Ashburner and Friston, 1999).  
169  $J_\varphi$  is the Jacobian matrix of the mapping function, whereas  $|J_\varphi|$  is the  
170 Jacobian determinant.  $W_i(\varphi(\mathbf{r}))$  are the diffusion signals acquired at  
171  $\varphi(\mathbf{r})$ .  $b_i$  is the b-value, and  $\hat{\mathbf{g}}_i$  is the direction of the diffusion sensitization  
172 gradient.  $\sigma$  is the diffusion sampling ratio controlling the detection

range of the diffusing spins.  $D$  is the diffusivity of water, and  $Z_0$  is the  
172 constant estimated by the diffusion signals of free water. 2 mm resolu-  
173 tion was assigned as the output resolution of the QSDR reconstruction  
174 for CMU and Brown University diffusion data, whereas the HCP data  
175 were reconstructed to 1 mm resolution. The SDFs of 60 subjects from  
176 CMU and 20 subjects from Brown University were averaged to create  
177 the CMU/BU-80 multisite atlas. The SDFs of HCP data at WU-Minn  
178 were averaged to construct the HCP-488 atlas. The SDF was sampled  
179 at a total of 642 sampling directions defined by an 8-fold tessellated  
180 icosahedron, and the local maxima (peaks) can be determined using  
181 the neighboring relation of the sampling directions. The peak directions  
182 on the averaged SDFs defined the local fiber directions that were used to  
183 measure the local connectomes in each subject. 184

### Local connectome matrix associated with study variables

For each voxel, the local fiber directions from a common diffusion  
186 MRI atlas provided the principle directions to sample the magnitudes  
187 of subject SDFs as the local connectome properties. The local  
188 connectomes of subjects were estimated by the density of anisotropic  
189 spins diffusing along the local fiber orientation (Fig. 3a): 190

$$\psi(\hat{a}) - iso(\psi) \quad (2)$$

where  $\psi$  is the SDF of the subject reconstructed by QSDR at a voxel, and  
192  $\hat{a}$  is the local fiber direction provided by a common dMRI atlas, and  
193  $iso(\psi)$  is the isotropic diffusion of the SDF estimated by taking the min-  
194 imum value of the SDF. The local connectomes of a subject were  
195 stretched into a row vector, and the vectors from a group of subjects  
196 were compiled into a single local connectome matrix (Fig. 3b). Each  
197 row of the matrix represents the local connectome of a subject, whereas  
198 each column corresponds to a common fiber direction from the atlas.  
199 The calculated local connectome matrix had a dimension of  $n$ -by- $m$ ,  
200 where  $n$  is the subject count and  $m$  is the total number of local  
201 connectome values. 202

A total of 59 CMU subjects had recorded body mass index (BMI)  
202 measures, and the local connectomes from these subjects were estimat-  
203 ed using Eq. (2), where the local fiber directions were identified from  
204 the CMU/BU 80 atlas. The local connectomes of these subjects were  
205 compiled into a local connectome matrix, where each row of the matrix  
206 represented the local connectome of a subject, and each column  
207 corresponded to each local fiber direction in the CMU/BU 80 atlas. We  
208 correlated the local connectome matrix with BMI, age, and sex using  
209 the following regression model (Fig. 2b): 210

$$\mathbf{Y} = \mathbf{XB} \quad (3)$$

where  $\mathbf{Y}$  is an  $n$ -by- $m$  local connectome matrix.  $n$  is the number of sub-  
212 jects, and  $m$  is the total number of local fiber directions in the dMRI atlas.  
213  $\mathbf{X}$  is an  $n$ -by-4 matrix, recording the BMI, age, and sex of each subject,  
214 and additional column is an all 1 vector for intercept.  $\mathbf{B}$  is a 4-by- $m$  co-  
215 efficient matrix. Since  $m > n$ ,  $\mathbf{B}$  can be calculated by a simple ordinary  
216 least square,  $(\mathbf{X}^\top \mathbf{X})^{-1} \mathbf{X}^\top \mathbf{Y}$ , and the first column of  $\mathbf{B}$ , denoted as  $\beta$  here-  
217 after, is a vector of coefficients corresponding to BMI. Since the row  
218 vectors of  $\mathbf{X}$  and  $\mathbf{Y}$  are independent to others, the empirical distribution  
219 of  $\mathbf{B}$  can be obtained by applying 5000 bootstrap resampling to the row  
220 vectors of matrix  $\mathbf{X}$ . Similarly, the null distribution of  $\mathbf{B}$  can be obtained  
221 by applying 5000 random permutations to the row vectors. 222

### Local connectomes and their statistical inference

The core hypothesis in connectometry is that the associations be-  
223 tween local connectomes and the study variables tend to propagate  
224 along a common fiber pathway. This hypothesis can be tested by track-  
225 ing local connectomes that express substantial association with BMI  
226 into a “track”, and comparing the length of this track with that from a  
227

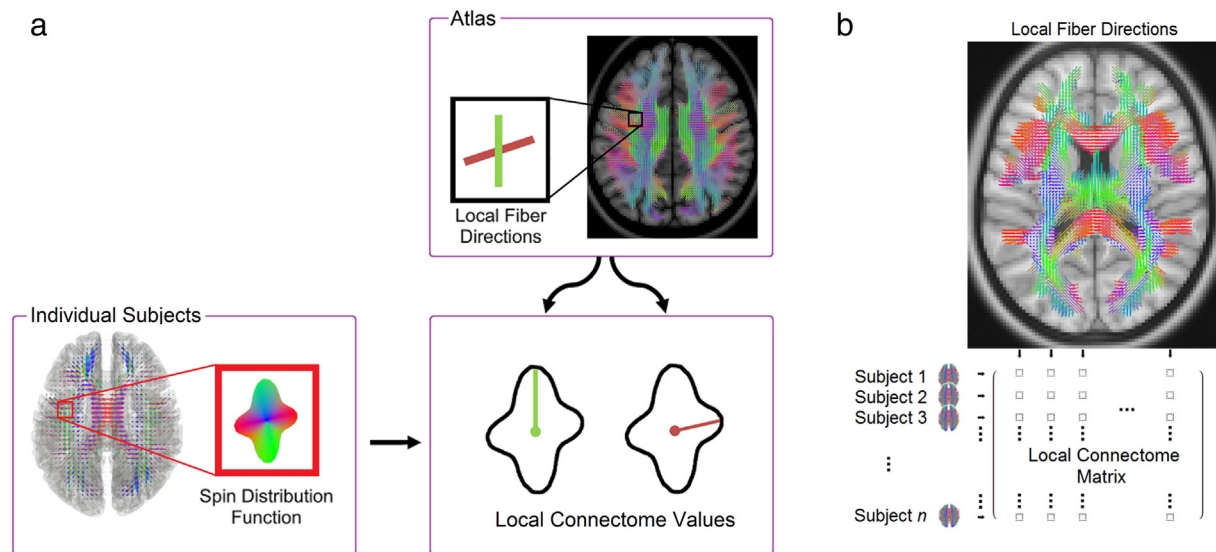


**Fig. 3.** (a) The magnitude of the spin distribution function at the fiber directions is used as the local connectome measurements. It is noteworthy that multiple fiber populations can coexist locally within a voxel, and each fiber population, identified by its fiber direction, has its unique local connectome estimation. (b) Compilation of a local connectome matrix from a group of subjects. The local connectome matrix provides an easy way to conduct statistical analysis on the local connectome. The local connectomes of each subject are arranged as a row vector in the matrix, and the vectors of a group of subjects can be compiled as a matrix. Since the rows are independent to each other, a distribution of this local connectome matrix can be generated by applying bootstrapping to the row vectors. Similarly, a null distribution can also be generated by randomly permuting the row vectors.

228 null distribution (Fig. 4). The positive and negative associations  
229 were studied separately. To study negative associations, the local  
230 connectomes with coefficients of less than a predefined negative  
231 threshold were filtered in, whereas for positive associations, the local  
232 connectomes with a coefficient value greater than a predefined thresh-  
233 old were filtered in. The predefined thresholds were automatically  
234 determined using Otsu's threshold (Otsu, 1979). This association pro-  
235 cedure identified local connectomes with substantial associations  
236 (colored sticks in Fig. 4), which may include true positive findings  
237 (red sticks) and false positive findings (blue sticks). The true positive  
238 findings (red sticks) could only be observed from the non-permuted  
239 local connectome matrix (lower row in Fig. 4), whereas the false posi-  
240 tive findings could be observed from both non-permuted and permuted

matrices. This allowed us to model the null distribution by randomly 241 permuting the local connectome matrix (upper row in Fig. 4). Using a 242 tracking algorithm (Yeh et al., 2013b), we placed a total of 10 seeds 243 per local connectome within its belonging voxel to start tracking. This 244 tracking procedure was conducted for a set of 5000 local connectome 245 matrices (without permutation) obtained from bootstrapping resam- 246 pling and another *null* set of 5000 local connectome matrices obtained 247 from random permutation. We formulated the null hypothesis for 248 each track as: the length of a track connected along substantial coeffi- 249 cients in the non-permuted condition is not longer than that from the 250 permuted condition. Since multiple tracks were connected throughout 251 the brain space, we used false discovery rate to reject the null hypoth- 252 eses and identified tracks with significant FDR. The length histograms of 253

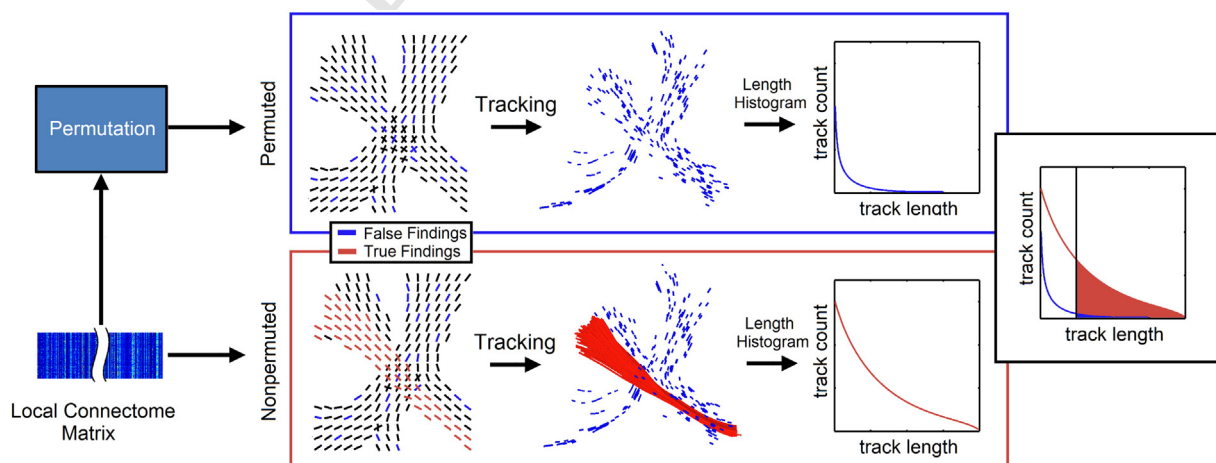


**Fig. 4.** Random permutation used to obtain the null distribution of the connectometry findings. The non-permuted local connectome matrix is regressed with the study variables (lower row), and the local connectomes that express associations can be visualized. The true findings (red sticks) tend to propagate along a common fiber pathway, whereas the false findings (blue sticks) are randomly distributed. The null distribution of the findings can be obtained by applying random permutation to the local connectome matrix (upper row). The permuted local connectome matrix is also regressed with the study variables to access the null distribution of the false findings (blue tracks). The tracks connected from false findings can be characterized by fragmented, short-ranged, tracks. By contrast, the true findings can be differentiated by its longer trajectories. Their difference can be quantified using a histogram of track length. We may view tracks with lengths greater than a threshold as true findings, and the false discovery rate can be calculated by the ratio of the area under the two distribution curves in the histogram.

254 the tracks were calculated, and the false discovery rate (FDR) of the  
 255 tracks in non-permuted condition were calculated by the ratio of the  
 256 area under the histogram curve.

257 In CMU 59 subjects' data, the FDR was controlled at 0.10, 0.075, and  
 258 0.05 to examine the results at different sensitivity/specificity levels. The  
 259 same analysis was repeated on 488 subjects (all had BMI information)  
 260 from the WU-Minn HCP Consortium to examine whether we could  
 261 obtain consistent results from two independently acquired data sets.

## 262 Comparison with connectivity matrix

263 The 59 CMU subjects with BMI data were reconstructed using gener-  
 264 alized q-sampling imaging (Yeh et al., 2010) with a length ratio of 1.25.  
 265 A total of 100,000 whole brain tracks were obtained using a fiber track-  
 266 ing algorithm (Yeh et al., 2013b). The default anisotropy threshold and  
 267 step size (determined automatically in DSI Studio) were used. The an-  
 268 gular threshold was 60°. The cortical parcellation was conducted by  
 269 warping the subject space to a standard space using non-linear registra-  
 270 tion (Ashburner and Friston, 1999). The cortex was partitioned using  
 271 the Automated Anatomical Labeling (AAL) atlas. A connectivity matrix  
 272 was calculated for each subject, and the entry of the matrix was the  
 273 mean quantitative anisotropy (QA) values of the corresponding tracks.  
 274 The connectivity matrices of 59 subjects were regressed with their  
 275 BMI, sex, and age using a linear regression model. The BMI-related coef-  
 276 ficients and uncorrected p-value can be calculated for each matrix entry  
 277 using a linear regression model. The false discovery rate of the uncor-  
 278 rected p-values was calculated using MATLAB (MathWorks, Inc.).

## 279 Comparison with tractography analysis

280 We chose the inferior longitudinal fasciculus (ILF) as the analysis  
 281 targets because it showed significant associations with BMI in the  
 282 connectometry analysis. The ILF was tracked on the CMU-BU 80 atlas  
 283 using the same fiber tracking algorithm (Yeh et al., 2013b), and the  
 284 QA values (Yeh et al., 2010) along the ILF were correlated with BMI,  
 285 age, and sex using a linear regression model. The T-score corresponding  
 286 to BMI were rendered on ILF to examine whether correlation was local-  
 287 ized. To test whether the connectivity at ILF was correlated with BMI,  
 288 the QA values at ILF were averaged for each subject and correlated  
 289 with BMI, age, and sex using a linear regression model. The scatter  
 290 plot of average QA values against BMI was generated for comparison,  
 291 and the p-value of the BMI association was calculated using the regres-  
 292 sion model.

## 293 Data analysis

294 The source code for connectometry described in this work is publicly  
 295 available at <https://github.com/frankyeh/DSI-Studio>, and the atlases  
 296 described in this paper can be downloaded from <http://dsi-studio.>  
 297 [labsolver.org](http://labsolver.org). The data analysis was conducted on a personal laptop  
 298 equipped with a 4.0 GHz quad-core CPU and 32 GB memory. A total  
 299 of 8 threads were used in computation. The CMU data (59 subjects,  
 300 2-mm resolution) used a total of 1B memory, and the computation  
 301 time was around 3 min, whereas the HCP data (488 subjects, 1-mm res-  
 302 olution) used a total of 18 GB memory, the computation time was  
 303 around 3 h.

## 304 Results

### 305 Local connectome associations

306 In order to illustrate the analytical potential of local connectomes,  
 307 we first show how study-relevant patterns can be identified along  
 308 local white matter fascicles in the CMU sample and follow up with a  
 309 replication of these findings in the HCP sample. The local connectome  
 310 matrix from the CMU sample is shown in Fig. 5. This illustrates the

311 large number of features (columns) relative to the number of samples  
 312 (rows). Local connectome values from the CMU subjects were then  
 313 regressed against BMI, sex, and age using linear regression. Consistent  
 314 with previous findings (Gianaros et al., 2013; Mueller et al., 2011;  
 315 Stanek et al., 2011; Verstynen et al., 2013, Verstynen et al., 2012), we  
 316 found many local connectomes that expressed a negative association  
 317 (i.e., decreased in local connectome as BMI increased) (Fig. 6a). These  
 318 local connectomes, termed negatively associated local connectomes,  
 319 appear to be distributed coherently along fiber bundles, supporting  
 320 the core hypothesis that patterns of variability tend to propagate  
 321 along a common fiber pathway. The negatively associated local  
 322 connectomes were then tracked using a fiber tracking algorithm, and  
 323 the tracking was restricted only to local connectome with substantial  
 324 associations determined by the Otsu's threshold, so as to reveal the sub-  
 325 components of fascicles that have negative associations with BMI  
 326 (Fig. 6b). The negative BMI associations are broadly distributed across  
 327 white matter pathways in a largely bilateral pattern. This result is con-  
 328 sistent with a previous study showing BMI's heterogeneous association  
 329 to white matter pathways across the brain (see Verstynen et al., 2013).

330 After identifying study-relevant associations, our next task was to  
 331 assess the statistical significance of these associations and to correct  
 332 for multiple comparisons. To do this we applied random permutations  
 333 to the row vectors of the local connectome matrix and recalculated its  
 334 association with BMI in order to visualize the null distribution of the  
 335 negatively associated local connectomes. As shown in the upper row  
 336 of Fig. 6c, these "null" local connectomes tend to be randomly distribut-  
 337 ed within white matter, and tracks connected from them are short-  
 338 distanced fragments that suggest poor continuity along the core fiber  
 339 pathways. This is substantially different from the non-permuted condi-  
 340 tion (lower row of Fig. 6c), where the negatively associated local  
 341 connectomes produce longer tracks. By repeating the random permuta-  
 342 tions 5000 times we can obtain a null distribution of track lengths if  
 343 associations to BMI were determined by chance. The true findings and  
 344 false findings can then be differentiated using a simple length thresh-  
 345 old and the false discovery rate (FDR) can be directly calculated from the  
 346 length histogram obtained from permuted and non-permuted condi-  
 347 tions. These length histograms allows for identifying the length thresh-  
 348 old that yields tracks with significant association ( $FDR < 0.05$ ).

349 To illustrate this, we calculated the length histograms for both posi-  
 350 tive and negative local connectome associations with BMI using the  
 351 CMU data set (Fig. 6d). The length histograms of negative associations  
 352 (local connectomes decrease as BMI increases) show substantial differ-  
 353 ences between the permuted and non-permuted distributions. Lengths  
 354 longer than 52, 42, and 31 mm correspond to FDRs of 0.05, 0.075, and  
 355 0.10, respectively. By contrast, the length histograms of positive associ-  
 356 ations (local connectomes increase as BMI increases) show substantial  
 357 overlap between permuted and non-permuted distributions, suggest-  
 358 ing that the positive association between local connectome and BMI  
 359 cannot be distinguished from random chance. We applied the same  
 360 connectometry analysis for BMI-associations in the 488 subjects in the  
 361 HCP sample. As with the CMU sample, the negative associations with  
 362 BMI were more frequent in the HCP sample than the positive associa-  
 363 tions. For the negatively associated local connectomes, lengths longer  
 364 than 14 mm correspond to an FDR of 0.05 (Fig. 6e), showing that a  
 365 large sample and a higher spatial resolution may increase the statistical  
 366 power of connectometry to detect finer structural associations.

367 Since statistical power varies with sample size, the FDR threshold  
 368 can be used to adjust the sensitivity and specificity of the  
 369 connectometry analysis when working with lower powered data.  
 370 Using the CMU data set as an example, a high FDR affords better sensi-  
 371 tivity for exploratory analysis, but it also increases false positive rates  
 372 (e.g.  $FDR < 0.1$  in Fig. 7a). A lower FDR offers a more specific result for  
 373 confirmation of the change in white matter structure; however, the  
 374 results may miss minor branches and has false negative results (e.g.  
 375  $FDR < 0.05$  in Fig. 7a). Thus, the FDR adjustment offers the flexibility  
 376 for different research purposes (e.g. exploratory or confirmative) by

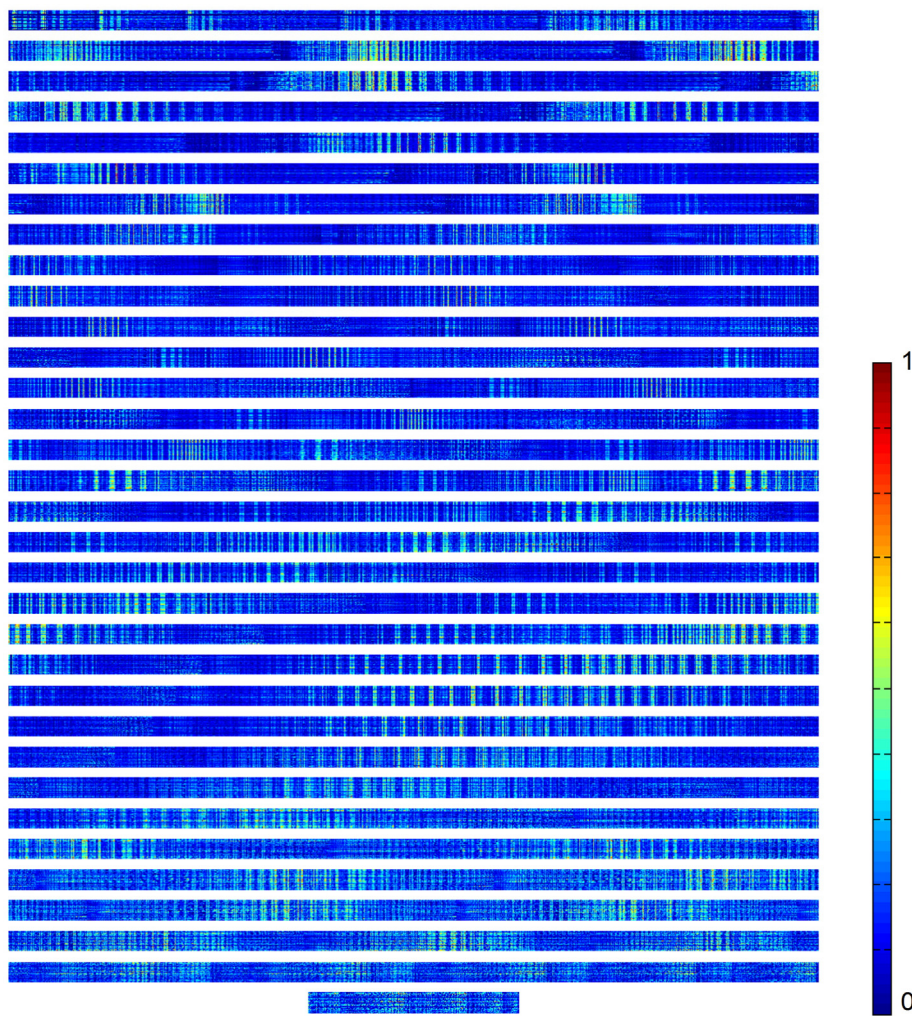


**Fig. 5.** The local connectome matrix of 59 subjects visualized. A local connectome matrix has a dimension of  $n$ -by- $m$ , where  $n$  is the number of subjects, and  $m$  is the number of local connectome, around 80,000 at 2-mm resolution and 900,000 at 1-mm resolution. The figure shows the matrix divided in multiple rows to facilitate visualization.

either controlling to a predefined threshold (e.g., 0.05) or using a predefined length threshold (e.g., >40 mm) and returning the FDR at that threshold. The FDR values can be affected by the image quality and the number of subjects included in the analysis. Using the HCP data set as an example, we show that with a larger subject pool and a higher spatial resolution, we may capture the associations in short-ranged connections as  $\text{FDR} < 0.05$  corresponds to lengths longer than 14 mm (Fig. 7b).

#### 385 Comparison with conventional diffusion MRI analyses

386 To illustrate how connectometry may complement conventional approaches, we applied variants of conventional end-to-end connectivity

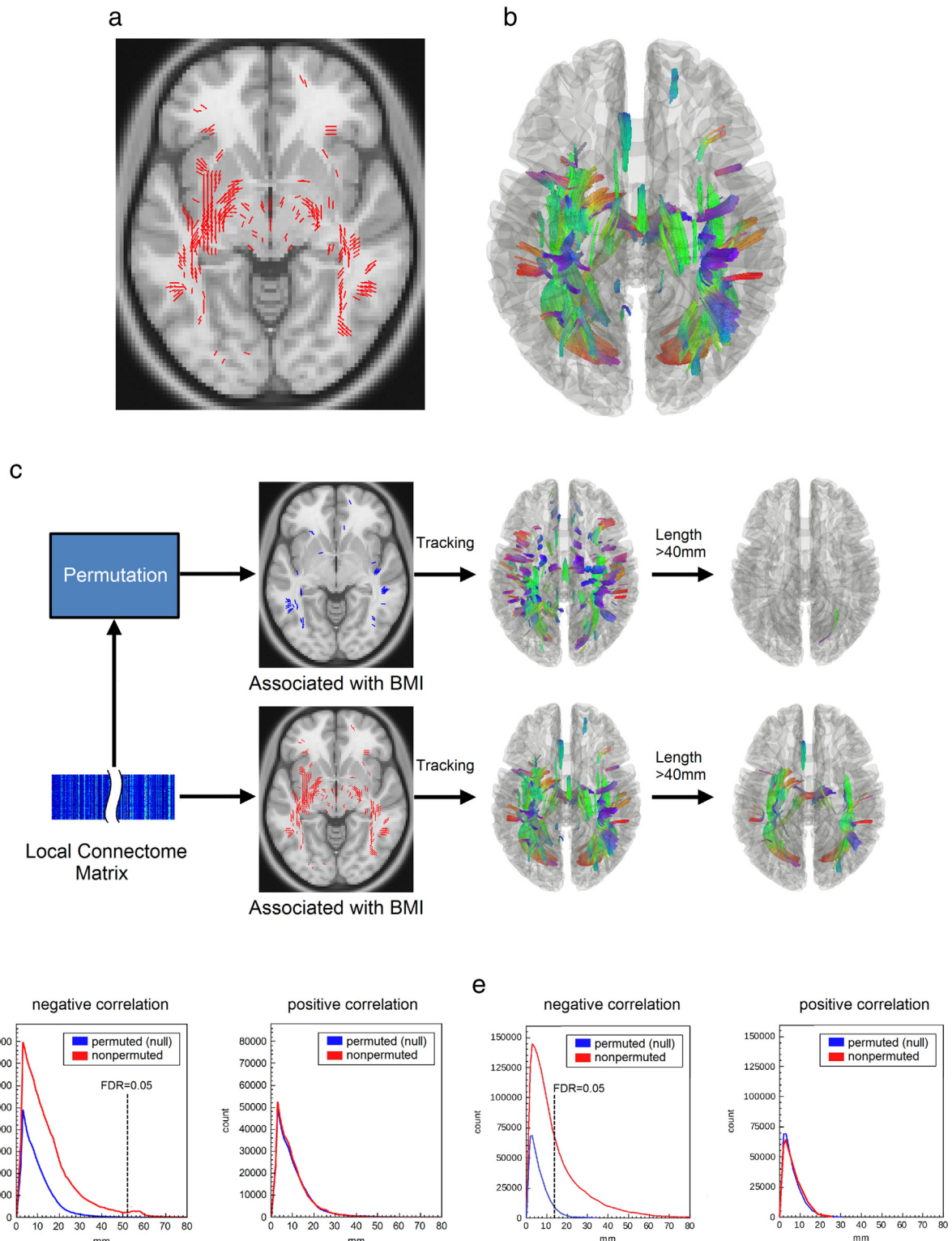
387 at gray matter targets (Hagmann et al., 2008, 2010a, 2010b). The con- 388 nection matrices of the CMU subjects were created using Automated 389 Anatomical Labeling (AAL) atlas for cortical parcellation and the mean 390 quantitative anisotropic (QA) value along the connecting trajectories 391 as the matrix entry. The connectivity matrices were regressed against 392 BMI, age, and sex using linear regression to produce a new matrix of 393 pairwise BMI-associations. Although the BMI-related coefficient matrix 394 in Fig. 8a shows no obvious correlation trend pattern between BMI and 395 the connectivity, the matrix has 79.52% of its non-zero entries being 396 negative, suggesting an overall negative correlation between BMI and 397 QA that is consistent with our connectometry results. The uncorrected 398 p-value map (Fig. 8b), in general, shows a greater significance level at 399 the intra-hemispheric connections (near the diagonal elements). 400

**Fig. 6.** The result of connectometry examined by a randomized permutation test. (a) The red sticks show local connectomes with substantial decrease of local connectome associated with high body mass index. The spatial distribution of these local connectomes follows the hypothesis that associations between local connectome patterns and study-relevant variables propagate along common fiber pathways. (b) A fiber tracking algorithm can be used to connect these local connectomes into tracks to reveal the subcomponent of fascicles that express associations. (c) The connectometry results can be statistically tested by a permutation test. The permuted (upper row) and non-permuted (lower row) local connectome matrices are associated with body mass index (BMI). Local connectomes that express negative associations with BMI are shown by colored sticks (blue: permuted red: non-permuted). These local connectomes can then be connected into "tracks" using a tracking algorithm to reveal the subcomponents of the fiber pathways that have negative associations. The non-permuted condition identifies several fiber pathways associated with BMI, whereas permuted local connectome matrix generates fragments of pathways. A simple length threshold can be applied to differentiate true and false findings. The false discovery rate can be calculated by the ratio of track count between non-permuted and permuted condition. (d) In 59-subject data set from CMU, the length histogram of tracks that express negative associations (non-permuted) is compared with the null distribution (permuted). The large discrepancy between two histogram curves suggests that there are tracks with a substantial decrease of local connectome due to BMI. The area ratio under two curves is false discovery rate of the findings. The same analysis is applied to study positive association with BMI. The length histogram shows substantial similarity between permuted and non-permuted conditions, suggesting that the positive associations between local connectome and BMI are no different from random effect. (e) In the 488-subject data set from WU-Min HCP, the length histogram of tracks that express negative associations (non-permuted) is compared with the null distribution (permuted). There is a large discrepancy between permuted and non-permuted conditions, suggesting a negative association with BMI. The positive associations between local connectome and BMI are no different from random effects.

401 However, the FDR of the most significant p-values is 0.1817, and an  
 402 alpha threshold of 0.05 will yield no significant pairwise associations  
 403 in the entire matrix, meaning that typical adjustments for multiple  
 404 comparisons would wipe out any BMI associations on end-to-end  
 405 connectivity. Nonetheless, the fact that BMI associates with individual  
 406 pairwise connections suggests that topological properties of the matrix  
 407 (e.g., associativity, centrality) also vary with BMI. This pattern of  
 408 end-to-end connectivity variation is consistent with the distributed  
 409 pathways identified in the connectometry analysis, suggesting that

connectometry provides complementary details about which sub- 410 components of connections within the fascicle are significantly asso- 411 ciated with BMI. 412

We also compared our connectometry results to typical 413 tractography-based region of interest analysis. The inferior longitudinal 414 fasciculus (ILF) was mapped using the CMU/BU 80 atlas, and the mean 415 QA values along ILF were regressed with BMI, age, and sex. The 416 ILF was chosen for illustrative purposes only due to its significant nega- 417 tive BMI associations in the connectometry analysis. The BMI-associated 418



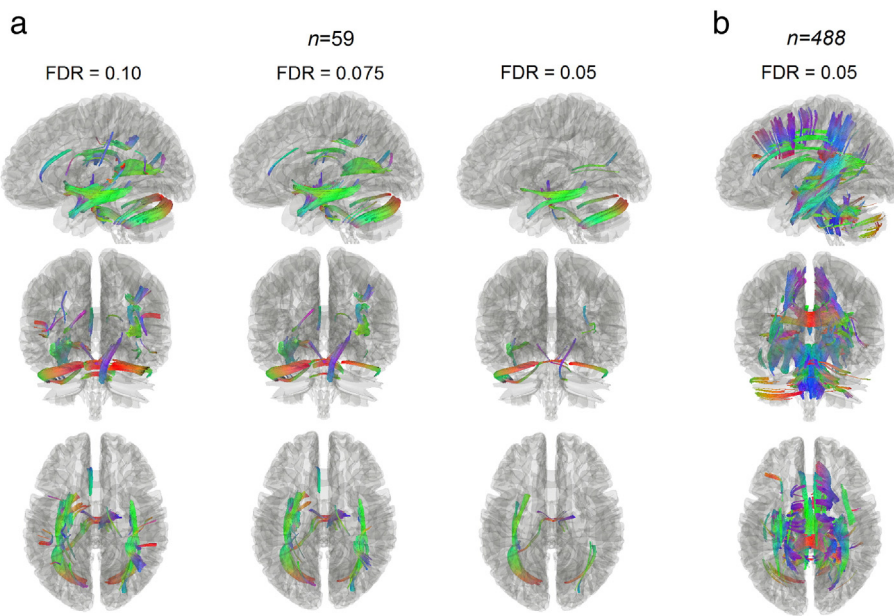


**Fig. 7.** Impact of FDR threshold and sample size on connectometry results. (a) The subjects from the CMU data set are analyzed by connectometry to reveal the subcomponents of fascicles that express negative associations with BMI. The false discovery rate (FDR) can be controlled to change the sensitivity and specificity of the findings. High FDR leads to more specific results but may miss true findings, while low FDR is more sensitive but may include false positive findings. (b) The HCP sample was analyzed by connectometry to reveal the subcomponents of fascicles that express negative associations with BMI. Inclusion of more study subjects allow for revealing smaller branches of fascicles that achieve significant associations.

t-statistics are rendered to the track bundle (Fig. 8c) in order to illustrate the degree of associations along the entire pathway. The anterior region of the ILF shows the strongest negative association with BMI, whereas the posterior segment shows weaker associations. This suggests that, within the region of interest, the magnitude of BMI associations varies substantially, making averaging across the ROI a conservative estimate of BMI–white matter associations. This is captured in the scatter plot in Fig. 8d, showing a negative association between BMI and the mean QA sampled across the entire ILF. As expected the relationship between BMI and mean QA is strong but not statistically significant ( $p = 0.06$ ). Thus, in this case, region-of-interest analysis is not sensitive enough to reveal the focal effect of BMI because it collapses across the entire fascicle and fails to consider regional variation in BMI associations within the pathway, whereas connectometry naturally isolates only the affected segment of the fascicle, thus achieving greater statistical sensitivity.

#### Discussion

Here we illustrate the analytical advantage of using the local connectome to identify white matter fascicles that express significant

study-related patterns of variability. While conventional connectome analyses are designed to find differences in whole fiber pathways, connectometry tracks the differences along the pathways themselves. Using data from two independent samples of subjects, scanned using different diffusion MRI approaches, we were able to identify subcomponents of many major white matter pathways associated with BMI. This also suggested that we can track statistically meaningful associations to identify subcomponents of white matter pathways associated with a particular variable of interest. We also show how the spatial specificity of connectometry can complement conventional end-to-end structural connectivity approaches (Hagmann et al., 2008; Rubinov and Sporns, 2010; Sporns et al., 2005). While the full connectivity matrix estimated from diffusion MRI tractography between gray matter targets catches large-scale associations at a network level, connectometry characterizes focal structural differences within the connected pathways that may drive any observed changes in connectivity. On the other hand, connectometry can be viewed as an alternative to conventional tractography-based region-of-interest analyses that aim to identify tracks first and then conduct analysis of anisotropy and diffusivity associated with the identified trajectories (Abhinav et al., 2014b; Jbabdi

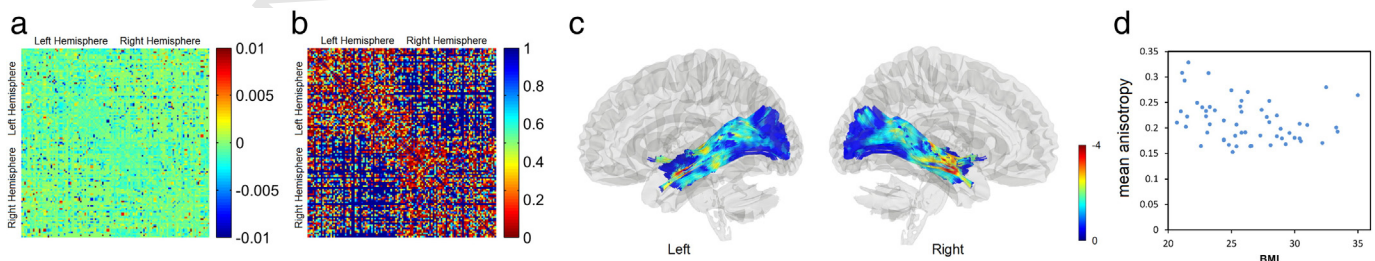


**Fig. 8.** Conventional connectome analysis applied to study BMI effect on white matter tracks. (a) The BMI-related coefficient matrix has 79.52% of its non-zero entries being negative, suggesting an overall trend of negative correlation between BMI and the connectivity. (b) The uncorrected p-value map shows that the intra-hemisphere connections have a greater significance level. (c) The t-statistics of BMI-related coefficients rendered on inferior longitudinal fasciculus show a focal effect of BMI on the fiber pathways. The structural change involves only a subcomponent of the entire fiber pathways. This suggests that the local connectome is a more suitable measurement to study the BMI effect on track integrity. (d) The scatter plot shows the mean anisotropy values of the fiber pathways against BMI. A linear regression model including age and sex is used to examine the correlation between the mean anisotropy value and BMI. The correlation is not significant ( $p\text{-value} = 0.06$ ). This demonstrates that tractography-based analysis is not power enough if the structure change involves only a segment of the fiber pathway.

and Johansen-Berg, 2011). The tractography-based analysis produces a more conservative estimate of white matter associations that sometimes inflates Type II error rates by averaging across many white matter voxels that may not have strong associations with the study variable of interest. By contrast, connectometry does not map the connectome itself. It analyzes difference in local connectome, associates local connectome with study variables, and then tracks the associations across a pathway. It is able to capture focal structural patterns in a sub-component of individual white matter fascicles, rather than the entire pathway itself. This provides a measure that is highly sensitive to regional variability in white matter and that can complement or inform graph-based connectomic analyses on the end-to-end connections.

Most diffusion MRI connectomics are conducted in a native subject space due to the methodological challenges in warping diffusion information to the stereotaxic space (Hagmann et al., 2010a, Hagmann et al., 2008, Hagmann et al., 2007, Hagmann et al., 2010b; Sporns et al., 2005). Connectometry bridges this gap by using q-space diffeomorphic reconstruction to reconstruct data directly in the stereotaxic space, allowing for integrating voxel-wise diffusion models (e.g., SDFs) across subjects and data sets (e.g. different diffusion schemes). This approach also allows for greater integration of structural analyses with functional imaging data analyzed in MNI-space, even in cases where fMRI data are collected on separate groups of subjects, opening the door to studying generalized structure–function relationships across studies.

Another advantage of connectometry is the atlas-based analysis in a standardized stereotaxic space. While atlas-based analysis has been the norm in fMRI for nearly two decades, there are only few studies using an atlas to analyze diffusion MRI measurements. Tract-based spatial statistics (TBSS) (Smith et al., 2006) uses a “skeleton” to analyze fractional anisotropy (FA), a diffusion index derived from a tensor model. The FA measure has been shown to reflect components of fiber integrity (Huisman et al., 2004; Werring et al., 2000), but studies have also shown that FA is susceptible to the partial volume of crossing fibers (Alexander et al., 2001, Alexander et al., 2002; Oouchi et al., 2007; Tuch et al., 2002; Yendiki et al., 2013). A more recent study used a fiber orientation distribution (FOD) template to analyze streamline count at each fiber direction (Raffelt et al., 2015), but whether stream count can be reliably correlated with the underlying anatomy has been put under question (Besseling et al., 2012; Jbabdi and Johansen-Berg, 2011; Jones et al., 2013). In comparison, connectometry uses the density of diffusion spins derived from a model free approach as the core diffusion measurement to reveal the compactness of fiber bundles (Yeh and Tseng, 2011; Yeh et al., 2013b). The density measurement is consistent across different diffusion schemes (Yeh and Tseng, 2013; Yeh et al., 2010, 2011), thus allowing connectometry to be applied to a variety of acquisition approaches, including conventional DTI, multi-shell diffusion images, and DSI. This feature is critical for comparing results across multiple studies and/or test sites. Connectometry also adopts a new paradigm—tracking the difference—to investigate the association of the diffusion measurement with a study variable. This paradigm is different from the conventional paradigm that seeks to map cortical connections (i.e. end-to-end connections) first and then study their associations. Mapping end-to-end connections has been a challenge due to methodological limitations (Jones et al., 2013; Reveley et al., 2015; Thomas et al., 2014), and a reliable and reproducible approach is still under active research. Connectometry bypasses this limitation by first quantifying the local associations and tracking only a subcomponent of the fiber pathway that expresses substantial association. The length of the affected subcomponent is used as the statistical index to help differentiate true findings from false findings caused by misalignment. Connectometry is also highly extensible to most regression frameworks due to the *independent and identically distributed* (i.i.d.) feature of the local connectome matrix. The ordinary least squares regression model used here can be replaced by sparse or non-linear regression approaches for more precise results. Also, non-regression metrics such as

group mean difference, paired difference, or percentile rank test can also be used to estimate the first state associations (Fig. 2b). Using different models, connectometry can examine associations between two groups of subjects, or to examine the change before and after a treatment, or to compare the connectivity differences between an individual with a normal population. Having a well characterized distribution of healthy normal variability in the normal local connectome could allow connectometry to be used to identify the white matter areas with pathological differences in clinical patients with neurological, psychological, and psychiatric disorders, providing a quantifiable and potential biomarker for white matter pathologies. While the initial concept of connectometry was proposed as a way of identifying pathological damage by comparing individuals with neurological damage to a normal population (Abhinav et al., 2014a, Abhinav et al., 2014b; Yeh et al., 2013a), here we extend the approach to include a regression model as a more general framework for group-wise, atlas-based comparison. This enables us to study the effect of BMI while also considering age and sex as the confounding factors. The extension can be applied to a large scale study that includes a complex set of demographic information to study the association between brain structure and a study variable.

In conclusion, we show how analyzing local connectomic patterns can be a powerful method for investigating variability in macroscopic white matter pathways. Connectometry can serve as a complementary approach for conventional structural connectomics. In the future, connectometry may further open the door to applying more sophisticated statistical models, such as machine learning classifiers, to investigate how brain structure associates with a study variable and highlights a rich clinical potential connectometry as a classifier for clinical pathologies.

## Uncited references

Q4

- Fernandez-Miranda et al., 2014 554
- Wang et al., 2013 555
- Yeatman et al., 2014 556

## Acknowledgments

557

Data were provided in part by the Human Connectome Project, WU-Minn Consortium (D. Van Essen and K. Ugurbil, 1U54MH091657 NIH). This research was sponsored by the Army Research Laboratory and was accomplished under Cooperative Agreement Number W911NF-10-2-0022 and NSF BIGDATA grant #1247658. The views and conclusions contained in this document are those of the authors and should not be interpreted as representing the official policies, either expressed or implied, of the Army Research Laboratory or the U.S. Government. The U.S. Government is authorized to reproduce and distribute reprints for Government purposes notwithstanding any copyright notation herein. This research was supported by an NSF BIGDATA Grant #1247658.

## References

570

- Abhinav, K., Yeh, F.C., El-Dokla, A., Ferrando, L.M., Chang, Y.F., Lacomis, D., Friedlander, R.M., Fernandez-Miranda, J.C., 2014a. Use of diffusion spectrum imaging in preliminary longitudinal evaluation of amyotrophic lateral sclerosis: development of an imaging biomarker. *Front. Hum. Neurosci.* 8, 270.
- Abhinav, K., Yeh, F.C., Pathak, S., Suski, V., Lacomis, D., Friedlander, R.M., Fernandez-Miranda, J.C., 2014b. Advanced diffusion MRI fiber tracking in neurosurgical and neurodegenerative disorders and neuroanatomical studies: a review. *Biochim. Biophys. Acta* 1842, 2286–2297.
- Akil, H., Martone, M.E., Van Essen, D.C., 2011. Challenges and opportunities in mining neuroscience data. *Science* 331, 708–712.
- Alexander, A.L., Hasan, K.M., Lazar, M., Tsuruda, J.S., Parker, D.L., 2001. Analysis of partial volume effects in diffusion-tensor MRI. *Magn. Reson. Med.* 45, 770–780.
- Alexander, D.C., Barker, G.J., Arridge, S.R., 2002. Detection and modeling of non-Gaussian apparent diffusion coefficient profiles in human brain data. *Magn. Reson. Med.* 48, 331–340.

- 586 Ashburner, J., Friston, K.J., 1999. Nonlinear spatial normalization using basis functions.  
587 Hum. Brain Mapp. 7, 254–266.
- 588 Besseling, R.M., Jansen, J.F., Overvliet, G.M., Vaessen, M.J., Braakman, H.M., Hofman, P.A.,  
589 Aldenkamp, A.P., Backes, W.H., 2012. Tract specific reproducibility of tractography  
590 based morphology and diffusion metrics. *PLoS One* 7, e34125.
- 591 Biswal, B.B., Mennes, M., Zuo, X.N., Gohel, S., Kelly, C., Smith, S.M., Beckmann, C.F.,  
592 Adelstein, J.S., Buckner, R.L., Colcombe, S., Dogonowski, A.M., Ernst, M., Fair, D.,  
593 Hampson, M., Hoptman, M.J., Hyde, J.S., Kiviniemi, V.J., Kotter, R., Li, S.J., Lin, C.P.,  
594 Lowe, M.J., Mackay, C., Madden, D.J., Madsen, K.H., Margulies, D.S., Mayberg, H.S.,  
595 McMahon, K., Monk, C.S., Mostofsky, S.H., Nagel, B.J., Pekar, J.J., Peltier, S.J., Petersen,  
596 S.E., Riedl, V., Rombouts, S.A., Rympma, B., Schlaggar, B.L., Schmidt, S., Seidler, R.D.,  
597 Siegle, G.J., Sorg, C., Teng, G.J., Veijola, J., Villringer, A., Walter, M., Wang, L., Weng,  
598 X.C., Whitfield-Gabrieli, S., Williamson, P., Windischberger, C., Zang, Y.F., Zhang,  
599 H.Y., Castellanos, F.X., Milham, M.P., 2010. Toward discovery science of human  
600 brain function. *Proc. Natl. Acad. Sci. U. S. A.* 107, 4734–4739.
- 601 Bullmore, E., Sporns, O., 2009. Complex brain networks: graph theoretical analysis of  
602 structural and functional systems. *Nat. Rev. Neurosci.* 10, 186–198.
- 603 Craddock, R.C., Jbabdi, S., Yan, C.G., Vogelstein, J.T., Castellanos, F.X., Di Martino, A., Kelly,  
604 C., Heberlein, K., Colcombe, S., Milham, M.P., 2013. Imaging human connectomes at  
605 the macroscale. *Nat. Methods* 10, 524–539.
- 606 DeFelipe, J., 2010. From the connectome to the synaptome: an epic love story. *Science*  
607 330, 1198–1201.
- 608 Dolgin, E., 2010. This is your brain online: the Functional Connectomes Project. *Nat. Med.*  
609 16, 351.
- 610 Fernandez-Miranda, J.C., Wang, Y., Pathak, S., Stefaneau, L., Verstynen, T., Yeh, F.C., 2014.  
611 Asymmetry, connectivity, and segmentation of the arcuate fascicle in the human  
612 brain. *Brain Struct. Funct.* 220, 1665–1680.
- 613 Fornito, A., Zalesky, A., Breakspear, M., 2015. The connectomics of brain disorders. *Nat.*  
614 *Rev. Neurosci.* 16, 159–172.
- 615 Gianaros, P.J., Marsland, A.L., Sheu, L.K., Erickson, K.I., Verstynen, T.D., 2013. Inflammatory  
616 pathways link socioeconomic inequalities to white matter architecture. *Cereb. Cortex*  
617 23, 2058–2071.
- 618 Hagmann, P., Kurant, M., Gigandet, X., Thiran, P., Wedeen, V.J., Meuli, R., Thiran, J.P., 2007.  
619 Mapping human whole-brain structural networks with diffusion MRI. *PLoS One* 2,  
620 e597.
- 621 Hagmann, P., Cammoun, L., Gigandet, X., Meuli, R., Honey, C.J., Wedeen, V.J., Sporns, O.,  
622 2008. Mapping the structural core of human cerebral cortex. *PLoS Biol.* 6, e159.
- 623 Hagmann, P., Cammoun, L., Gigandet, X., Gerhard, S., Grant, P.E., Wedeen, V., Meuli, R.,  
624 Thiran, J.P., Honey, C.J., Sporns, O., 2010a. MR connectomics: principles and chal-  
625 lenges. *J. Neurosci. Methods* 194, 34–45.
- 626 Hagmann, P., Sporns, O., Madan, N., Cammoun, L., Pienaar, R., Wedeen, V.J., Meuli, R.,  
627 Thiran, J.P., Grant, P.E., 2010b. White matter maturation reshapes structural connec-  
628 tivity in the late developing human brain. *Proc. Natl. Acad. Sci. U. S. A.* 107,  
629 19067–19072.
- 630 Honey, C.J., Sporns, O., Cammoun, L., Gigandet, X., Thiran, J.P., Meuli, R., Hagmann, P.,  
631 2009. Predicting human resting-state functional connectivity from structural connec-  
632 tivity. *Proc. Natl. Acad. Sci. U. S. A.* 106, 2035–2040.
- 633 Huisman, T.A., Schwamm, L.H., Schaefer, P.W., Koroshetz, W.J., Shetty-Alva, N., Ozsunar,  
634 Y., Wu, O., Sorensen, A.G., 2004. Diffusion tensor imaging as potential biomarker of  
635 white matter injury in diffuse axonal injury. *AJNR Am. J. Neuroradiol.* 25, 370–376.
- 636 Jbabdi, S., Johansen-Berg, H., 2011. Tractography: where do we go from here? *Brain Con-*  
637 *nnect.* 1, 169–183.
- 638 Johansen-Berg, H., Behrens, T.E., Robson, M.D., Drobniak, I., Rushworth, M.F., Brady, J.M.,  
639 Smith, S.M., Higham, D.J., Matthews, P.M., 2004. Changes in connectivity profiles de-  
640 fine functionally distinct regions in human medial frontal cortex. *Proc. Natl. Acad. Sci.*  
641 *U. S. A.* 101, 13335–13340.
- 642 Jones, D.K., Knosche, T.R., Turner, R., 2013. White matter integrity, fiber count, and other  
643 fallacies: the do's and don'ts of diffusion MRI. *NeuroImage* 73, 239–254.
- 644 Mueller, K., Anwander, A., Moller, H.E., Horstmann, A., Lepsius, J., Busse, F., Mohammadi,  
645 S., Schroeter, M.L., Stumvoll, M., Villringer, A., Pleyer, B., 2011. Sex-dependent influ-  
646 ences of obesity on cerebral white matter investigated by diffusion-tensor imaging.  
647 *PLoS One* 6, e18544.
- 648 Nichols, T.E., Holmes, A.P., 2002. Nonparametric permutation tests for functional neuro-  
649 imaging: a primer with examples. *Hum. Brain Mapp.* 15, 1–25.
- 650 Ouchi, H., Yamada, K., Sakai, K., Kizu, O., Kubota, T., Ito, H., Nishimura, T., 2007. Diffusion  
651 anisotropy measurement of brain white matter is affected by voxel size: underesti-  
652 mation occurs in areas with crossing fibers. *AJNR Am. J. Neuroradiol.* 28, 1102–1106.
- 653 Otsu, N., 1979. A threshold selection method from gray-level histograms. *IEEE Trans. Syst.*  
654 *Man Cybern.* 9, 62–66.
- 655 Pestilli, F., Yeatman, J.D., Rokem, A., Kay, K.N., Wandell, B.A., 2014. Evaluation and statisti-  
656 cal inference for human connectomes. *Nat. Methods* 11, 1058–1063.
- 657 Raffelt, D.A., Smith, R.E., Ridgway, G.R., Tournier, J.D., Vaughan, D.N., Rose, S., Henderson,  
658 R., Connelly, A., 2015. Connectivity-based fixel enhancement: whole-brain statistical  
659 analysis of diffusion MRI measures in the presence of crossing fibres. *NeuroImage* 659  
660 117, 40–55.
- 661 Reveley, C., Seth, A.K., Pierpaoli, C., Silva, A.C., Yu, D., Saunders, R.C., Leopold, D.A., Ye, F.Q.,  
662 2015. Superficial white matter fiber systems impede detection of long-range cortical  
663 connections in diffusion MR tractography. *Proc. Natl. Acad. Sci. U. S. A.* 112, 663  
664 E2820–E2828.
- 665 Rubinov, M., Sporns, O., 2010. Complex network measures of brain connectivity: uses and  
666 interpretations. *NeuroImage* 52, 1059–1069.
- 667 Seung, H.S., 2011. Neuroscience: towards functional connectomics. *Nature* 471, 170–172.
- 668 Smith, S.M., Jenkinson, M., Johansen-Berg, H., Rueckert, D., Nichols, T.E., Mackay, C.E.,  
669 Watkins, K.E., Ciccarelli, O., Cader, M.Z., Matthews, P.M., Behrens, T.E., 2006. Tract-  
670 based spatial statistics: voxelwise analysis of multi-subject diffusion data. *NeuroImage* 31,  
671 1487–1505.
- 672 Sotiropoulos, S.N., Jbabdi, S., Xu, J., Andersson, J.L., Moeller, S., Auerbach, E.J., Glasser, M.F.,  
673 Hernandez, M., Sapir, G., Jenkinson, M., Feinberg, D.A., Yacoub, E., Lenglet, C., Van  
674 Essen, D.C., Ugurbil, K., Behrens, T.E., 2013. Advances in diffusion MRI acquisition  
675 and processing in the Human Connectome Project. *NeuroImage* 80, 125–143.
- 676 Sporns, O., 2013. The human connectome: origins and challenges. *NeuroImage* 80, 53–61.
- 677 Sporns, O., 2014a. Contributions and challenges for network models in cognitive neuro-  
678 science. *Nat. Neurosci.* 17, 652–660.
- 679 Sporns, O., 2014b. Towards network substrates of brain disorders. *Brain* 137, 2117–2118.
- 680 Sporns, O., Tononi, G., Kotter, R., 2005. The human connectome: a structural description of  
681 the human brain. *PLoS Comput. Biol.* 1, e42.
- 682 Stanek, K.M., Grieve, S.M., Brickman, A.M., Korgaonkar, M.S., Paul, R.H., Cohen, R.A.,  
683 Gunstad, J.J., 2011. Obesity is associated with reduced white matter integrity in oth-  
684 erwise healthy adults. *Obesity (Silver Spring)* 19, 500–504.
- 685 Thomas, C., Ye, F.Q., Irfanoglu, M.O., Modi, P., Saleem, K.S., Leopold, D.A., Pierpaoli, C., 2014.  
686 Anatomical accuracy of brain connections derived from diffusion MRI tractography is  
687 inherently limited. *Proc. Natl. Acad. Sci. U. S. A.* 111, 16574–16579.
- 688 Tuch, D.S., Reese, T.G., Wiegell, M.R., Makris, N., Belliveau, J.W., Wedeen, V.J., 2002. High  
689 angular resolution diffusion imaging reveals intravoxel white matter fiber heteroge-  
690 neity. *Magn. Reson. Med.* 48, 577–582.
- 691 Turk-Browne, N.B., 2013. Functional interactions as big data in the human brain. *Science*  
692 342, 580–584.
- 693 Verstynen, T.D., Weinstein, A.M., Schneider, W.W., Jakicic, J.M., Rofey, D.L., Erickson, K.I.,  
694 2012. Increased body mass index is associated with a global and distributed decrease  
695 in white matter microstructural integrity. *Psychosom. Med.* 74, 682–690.
- 696 Verstynen, T.D., Weinstein, A., Erickson, K.I., Sheu, L.K., Marsland, A.L., Gianaros, P.J., 2013.  
697 Competing physiological pathways link individual differences in weight and abdom-  
698 inal adiposity to white matter microstructure. *NeuroImage* 79, 129–137.
- 699 Wang, Y., Fernandez-Miranda, J.C., Verstynen, T., Pathak, S., Schneider, W., Yeh, F.C., 2013.  
700 Rethinking the role of the middle longitudinal fascicle in language and auditory path-  
701 ways. *Cereb. Cortex* 23, 2347–2356.
- 702 Wedeen, V.J., Rosene, D.L., Wang, R., Dai, G., Mortazavi, F., Hagmann, P., Kaas, J.H., Tseng,  
703 W.Y., 2012. The geometric structure of the brain fiber pathways. *Science* 335, 703  
1628–1634.
- 704 Werring, D.J., Toosy, A.T., Clark, C.A., Parker, G.J., Barker, G.J., Miller, D.H., Thompson, A.J.,  
705 2000. Diffusion tensor imaging can detect and quantify corticospinal tract degenera-  
706 tion after stroke. *J. Neurol. Neurosurg. Psychiatry* 69, 269–272.
- 707 Yeatman, J.D., Weiner, K.S., Pestilli, F., Rokem, A., Mezer, A., Wandell, B.A., 2014. The ver-  
708 tical occipital fasciculus: a century of controversy resolved by *in vivo* measurements.  
709 *Proc. Natl. Acad. Sci. U. S. A.* 111, E5214–E5223.
- 710 Yeh, F.C., Tseng, W.Y., 2011. NTU-90: a high angular resolution brain atlas constructed by  
711 q-space diffeomorphic reconstruction. *NeuroImage* 58, 91–99.
- 712 Yeh, F.C., Tseng, W.Y., 2013. Sparse solution of fiber orientation distribution function by  
713 diffusion decomposition. *PLoS One* 8, e75747.
- 714 Yeh, F.C., Wedeen, V.J., Tseng, W.Y., 2010. Generalized q-sampling imaging. *IEEE Trans.*  
715 *Med. Imaging* 29, 1626–1635.
- 716 Yeh, F.C., Wedeen, V.J., Tseng, W.Y., 2011. Estimation of fiber orientation and spin density  
717 distribution by diffusion deconvolution. *NeuroImage* 55, 1054–1062.
- 718 Yeh, F.C., Tang, P.F., Tseng, W.Y., 2013a. Diffusion MRI connectometry automatically  
719 reveals affected fiber pathways in individuals with chronic stroke. *NeuroImage Clin.* 2,  
720 912–921.
- 721 Yeh, F.C., Verstynen, T.D., Wang, Y., Fernandez-Miranda, J.C., Tseng, W.Y., 2013b. Deter-  
722 ministic diffusion fiber tracking improved by quantitative anisotropy. *PLoS One* 8,  
723 e80713.
- 724 Yendiki, A., Koldewyn, K., Kakunoori, S., Kanwisher, N., Fischl, B., 2013. Spurious group  
725 differences due to head motion in a diffusion MRI study. *NeuroImage* 88C, 79–90.